Liquid Crystals
Publication details, including instructions for authors and subscription information:
http://www.informaworld.com/smpp/title~content=t713926090

Thermal switching characteristics based on smectic-A↔chiral nematic phase transitions of (liquid crystals/chiral dopant) composites, with and without side chain-type liquid crystalline polymer

Huai Yang; Hirotsugu Kikuchi; Tisato Kajiyama

Online publication date: 11 November 2010

To cite this Article Yang, Huai , Kikuchi, Hirotsugu and Kajiyama, Tisato(2002) 'Thermal switching characteristics based on smectic-A↔chiral nematic phase transitions of (liquid crystals/chiral dopant) composites, with and without side chain-type liquid crystalline polymer', Liquid Crystals, 29: 9, 1141 — 1149
To link to this Article: DOI: 10.1080/02678290210160105
URL: http://dx.doi.org/10.1080/02678290210160105

LIQUID CRYSTALS, 2002, VOL. 29, NO. 9, 1141–1149

Thermal switching characteristics based on smectic-A ↔ chiral nematic phase transitions of (liquid crystals/chiral dopant) composites, with and without side chain-type liquid crystalline polymer

HUAI YANG, HIROTSUGU KIKUCHI

Department of Applied Chemistry, Faculty of Engineering, Kyushu University, 6-10-1 Hakozaki, Higashi-ku, Fukuoka 812-8581, Japan

and TISATO KAJIYAMA*

Kyushu University, 6-10-1 Hakozaki, Higashi-ku, Fukuoka 812-8581, Japan

(*Received 10 December 2001; in final form 10 April 2002; accepted 15 April 2002*)

The light switching characteristics induced by a thermal smectic A (SmA)↔chiral nematic (N*) phase transition were studied for homeotropically aligned [smectic A liquid crystal (SmA-LC)/nematic liquid crystal (N-LC)/chiral dopant] and [side chain type smectic A liquid crystalline polymer (SmA-LCP)/N-LC/chiral dopant] composites. A drastic change from a transparent SmA phase to a light-scattering N* phase occurred in both composites upon heating. In the case of the heat-induced N* phase for the (SmA-LC/N-LC/chiral dopant) composite, the N* phase exhibited weak light scattering due to formation of a scroll texture. On the other hand, in the case of the heat-induced N* phase for the (SmA-LCP/N-LC/chiral dopant) composite, the N* phase showed strong light scattering due to formation of a focal-conic texture. The existence of a SmA-LCP was responsible for a higher contrast ratio between the transparent SmA phase and the light scattering N* phase for the (SmA-LCP/N-LC/chiral dopant) composite than for the (SA-LCN/N-LC/chiral dopant) composite.

1. Introduction

Since thermotropic side chain-type liquid crystalline polymers (SCLCPs) exhibit both inherent mesomorphic properties of liquid crystals (LCs) and excellent mechanical characteristics of polymer materials, they have attracted much attention due to their promising application in electro-optical devices [1]. However, the primary disadvantage of SCLCPs in a mesophase state is their higher viscosity than LCs. Since LCs can take the role of solvent or diluent to SCLCPs to reduce their viscosity, (SCLCP/LC) composites have significant potential as a novel type of LC material [2, 3]. Moreover, it has been reported that the (SCLCP/LC) composite exhibits some unique characteristics which are not found in the cases of individual SCLCPs or LCs [4–14].

As a novel and unique characteristic, a reversible and bistable electro-optical effect based on light scattering has been recognized for a smectic phase of an (SCLCP/LC) composite [3, 6]. In the case of the smectic (SCLCP/LC) composite, a light scattering state appeared upon application of an a.c. electric field below a threshold frequency (f_c). The light scattering state of the smectic (SCLCP/LC) composite occurred as a result of a random orientational distribution of smectic domain fragments, induced mainly by an electric current effect based on an electro-hydrodynamic motion of the backbones of the SCLCP. Therefore, the light scattering intensity of the (SCLCP/LC) composite in the SmA phase was much stronger than that of the SmA-LC itself, due to an enhanced random orientational distribution of smectic domain fragments. Thus, the light scattering intensity of a LC could be enhanced remarkably by mixing a SCLCP with a LC.

Recently, it has been reported that the homeotropically aligned (SCLCP/LC/chiral dopant) composite exhibits an extremely sharp change from a transparent homeotropic state of the SmA phase to a strong light scattering focal-conic state of the N* phase due to the heat-induced SmA → N* phase transition. When the composite system was slowly cooled from the heat-induced light scattering N* phase to the SmA phase, the SmA phase turned into a homeotropic monodomain and became transparent again. On the other hand, in

*Author for correspondence;
e-mail: tkajitcf@mbox.nc.kyushu-u.ac.jp

Liquid Crystals ISSN 0267-8292 print/ISSN 1366-5855 online © 2002 Taylor & Francis Ltd
http://www.tandf.co.uk/journals
DOI: 10.1080/02678290210160105

the case of rapid cooling of the composite system, the SmA phase retained a strong light scattering state. Also, when an a.c. electric field above a threshold value was applied to the light scattering SmA phase, it was changed to the transparent SmA phase in a monodomain state.

The thermally and electrically induced transparent–light scattering change for the (SCLCP/LC/chiral dopant) composite leads us to expect that thermal and electrical light switching may be applicable as a promising thermally addressable and electrically erasable liquid crystal display (TAEELCD), with a much greater speed for memory switching compared with the conventional TAEELCD. Meanwhile, this novel TAEELCD also exhibited a higher contrast and a more endurable memory effect than the conventional one [11, 12]. Furthermore, the latent heat of the SmA $\rightarrow$ N* phase transition is very small in general, since the transition is very weak first or second order. Therefore, the change from the transparent to the light scattering state corresponding to the SmA $\rightarrow$ N* transition can be induced by low power laser energy [13, 14].

In order to understand an additional effect of the SCLCP on the thermo-electro-optical properties of the (SCLCP/LC/chiral dopant) composite system, the thermal light switching characteristics induced by the SmA $\leftrightarrow$ N* phase transition have been investigated for the (SmA-LC/N-LC/chiral dopant) and the (SmA-SCLCP/N-LC/chiral dopant) composites.

2. Experimental

2.1. *Materials*

The SmA-SCLCP [PS(4BC/DM)], an N-LC (E7), an SmA-LC (S2) and a chiral dopant (CB-15) were used as component materials of the composite. E7, S2 and CB-15 were purchased from Merck Co., Ltd. The chemical structure and some physical properties of these materials are shown in figure 1. PS (4BC/DM) was synthesized by the method proposed by Finkelmann *et al.* [15]. The purity and the molecular weight of PS(4BC/DM) were measured by GPC, and the block ratio was determined by NMR and FTIR. The (S2/E7/CB-15) and the [PS(4BC/DM)/E7/CB-15] composites were prepared by a solvent cast method from acetone solutions.

2.2. *Characterization of composites*

The phase transition temperatures and aggregation structure of the (S2/E7/CB-15) and [PS(4BC/DM)/E7/CB-15] composites were investigated by differential scanning calorimetry (DSC), polarizing optical microscopy (POM) and wide angle X-ray diffraction (WAXD) studies. DSC thermograms were obtained with a Rigaku DSC8230B instrument at a heating rate of 5.0 K min^{-1} under a dry nitrogen purge. POM observations under crossed Nicol prisms were made using a Nikon polarizing

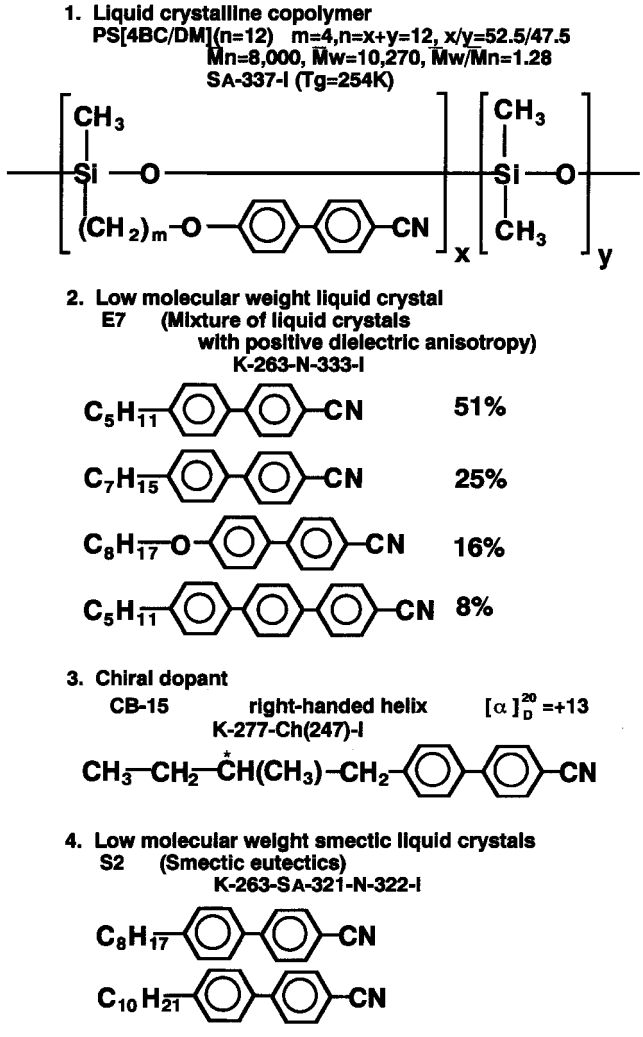

Figure 1. Chemical structure and physical properties of the materials used.

optical microscope equipped with a hot stage calibrated to an accuracy ± 0.05 K. WAXD studies were carried out using Ni filtered Cu K_α ($\lambda = 0.15405$ nm) radiation from a M18XHF (Macscience Co., Ltd.) X-ray generator.

2.3. *Treatment of homeotropic orientation*

The inner surfaces of the cells, made of indium tin oxide (ITO) coated glass substrates, were chemically treated to provide a homeotropic alignment of LC molecules with dimethyloctadecyl[3-(trimethoxysilyl)-propyl]ammonium chloride (DMOAP, Fluka Co., Ltd.) using the method proposed by Kahn [16].

2.4. *Fabrication of cells*

Poly(ethylene terephthalate) (PET) films of 14 μm thickness were used as cell spacers to keep the cell gap constant, and the composites were filled into the cells by capillary action in their isotropic (I) phases.

2.5. *Measurements of pitch lengths*

The Cano-Wedge technique [17] was used to measure the pitch lengths of the N* phases for the composites. In this measurement, a wedge-shaped cell with a wedge angle, α, was used and the inner surfaces of its two glass substrates were treated to provide a homogeneous alignment of LC molecules. To obtain homogeneous alignment, a 3.0 wt % polyvinyl alcohol (PVA) aqueous solution was coated onto the ITO-coated surfaces by spinning casting. The deposited film was dried at 353.2 K for about 30 min, and subsequently rubbed with a textile cloth under a pressure of 2.0 g cm^{-2} along one direction. After the composite was filled into the cell in the isotropic phase and then cooled to the N* phase, at some temperature a Grandjean–Cano texture formed with disclination lines separated by a distance l. Then the pitch length P is expressed by $P = 2l\alpha$ at that temperature.

2.6. *Measurements of thermo-optical effects*

The temperature and applied electric field dependences of the light transmittance for the composites were obtained as schematically shown in figure 2. A He-Ne laser (2 mW, 632.8 nm) beam was used as an incident light and the intensity of the transmitted light was recorded with a photodiode. The transmittance of a blank cell was normalized as 100%.

2.7. *Laser diffraction experiments*

Figure 3 shows the experimental set-up for laser diffraction measurements for detection of the Bragg diffraction from the helical structure in the composite.

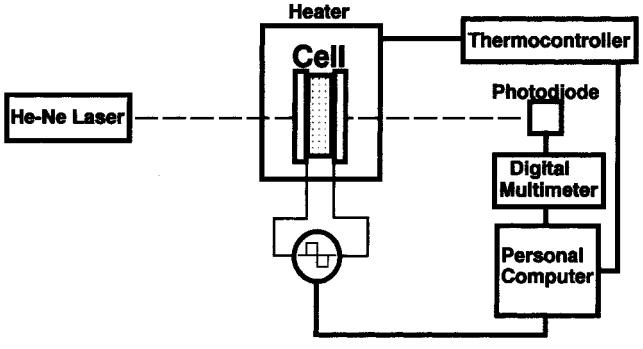

Figure 2. Schematic representation of experimental set-up to measure thermo-electro-optical properties of the composites.

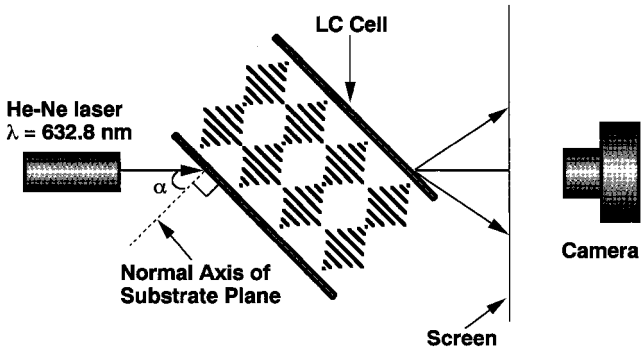

Figure 3. Schematic representation of experimental set-up for measurement of laser diffraction properties of the composites.

A He-Ne laser beam (2 mW, 632.8 nm) was used as the incident light. The laser beam was incident on the cell at angle α which was the angle between the laser beam line and the normal axis of the substrate surface. The screen plane, for projection of the diffracted light spots from the cell, was placed perpendicular to the laser beam. Photographs of the diffracted pattern projected on the screen were taken by a camera.

3. Results and discussion

The table lists the composite codes, their compositions, phase transition temperatures, pitch lengths of the N* phases and the thicknesses of the cell spacers for samples A and B. The SmA $\leftrightarrow$ N* transition point and the SmA temperature range of the samples are important in this study because thermo-optical switching is performed by heating above the SmA $\leftrightarrow$ N* transition point, and the characters recorded by thermo-optical switching are stored in the SmA phase. The phase transition temperature of the materials used in this study can be adjusted to a certain extent by controlling the composition ratios of (SmA-LC/N-LC) and (SmA-SCLCP/N-LC). For convenience in the thermo-optical experiments, the SmA phase region was adjusted to be close to room temperature (285 $\sim$ 300 K), and the SmA $\leftrightarrow$ N* transition temperature was adjusted to be 5 $\sim$ 10 K higher than room temperature. In general, SCLCPs have a strong tendency to stabilize the smectic phase in the composite because of the comb-like molecular shape. Therefore, in the case of compositions (SmA-LC/N-LC/chiral dopant) and

Table 1. Codes, compositions, phase transition temperatures, pitch lengths of the N* phases and thicknesses of the spacers of the cells for samples A and B.

Sample	Code	Composition/wt %	Phase transition temperature/K	Pitch length/μm	Thickness of the cell spacer/μm
A	S2/E7/CB-15	61.9/33.3/4.8	Cr 266.3 SmA 303.0 N* 323.8 I	3.4	15
B	PS(4BC/DM)/E7/CB-15	33.3/61.9/4.8	g 220.5 SmA 309.5 N* 327.2 I	3.6	18

(SmA-SCLCP/N-LC/chiral dopant), the former composite needs a higher fraction of the SmA component than the latter for adjusting the SmA↔N* transition temperature to be the same. Sample A shown in table 1 was composed of S2, E7 and CB-15 which are low molecular mass substances, while sample B included a polymeric substance, PS(4BC/DM) as a SmA-SCLCP. The fraction of SmA-LC in sample A was adjusted to be considerably larger than that of SmA-SCLCP in sample B.

Figures 4 and 5 show the temperature dependences of the transmittance for samples A and B, respectively. Figures 6 and 7 show, respectively, the POM observation photographs taken at 298.2 K for samples A and B in the smectic state. Since the inner surfaces of the cell substrates sandwiching samples A and B were treated homeotropically, the optic axis (i.e. the director) of the LC molecules, or the mesogenic groups in the SmA phase, were oriented in the direction perpendicular to the substrate surfaces in a single crystal manner, due to the anchoring effect of the surface orientation agent. Therefore, samples A and B in the SmA phase formed an optically uniform monodomain with the homeotropic molecular alignment and were optically isotropic for the ray of incident light along the substrate surface normal. Thus samples A and B in the temperature ranges of their SmA phases showed a dark field by POM observation under crossed Nicols, as shown in figures 6 and 7, and had high transmittances as shown in figures 4 and 5 (curves 1 and 2), respectively. Figures 4 and 5 also show that the transmittances began to decrease

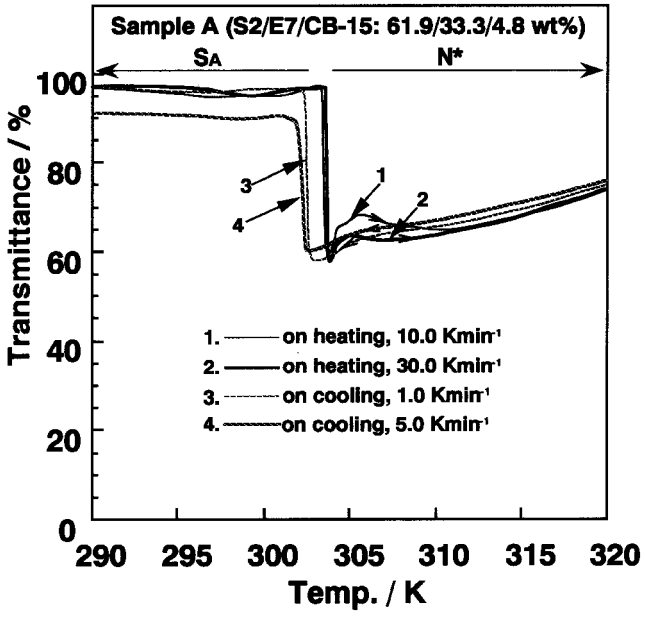

Figure 4. Plots of temperature versus transmittance for sample A.

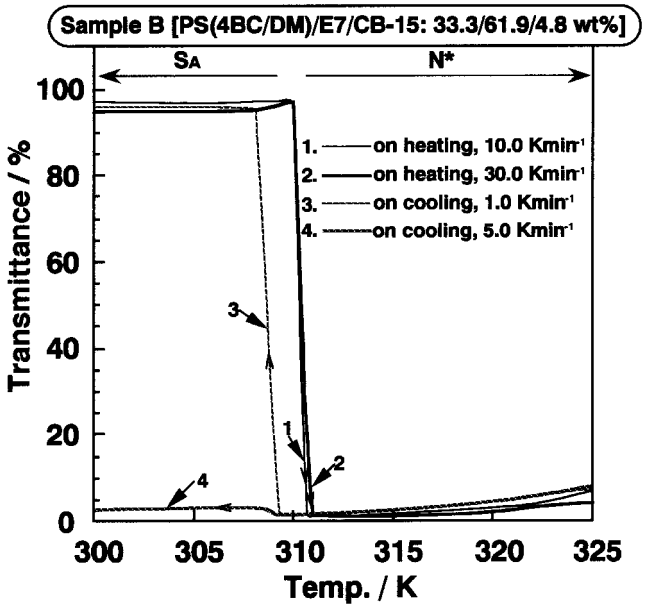

Figure 5. Plots of temperature versus transmittance for sample B.

Figure 6. POM photomicrograph of the texture of the SmA phase for Sample A taken at 298.2 K.

strikingly due to the appearance of light scattering at the heat-induced SmA→N* transition points upon heating the samples A and B. The temperature range of the sharp transmittance change between the transparent SmA and the light scattering N* phases was narrower than 1.0 K.

It is apparent from a comparison between figures 4 and 5 that the light scattering intensity of the heat-induced N* phase for sample B was much stronger than that for sample A. To determine the reason for such a

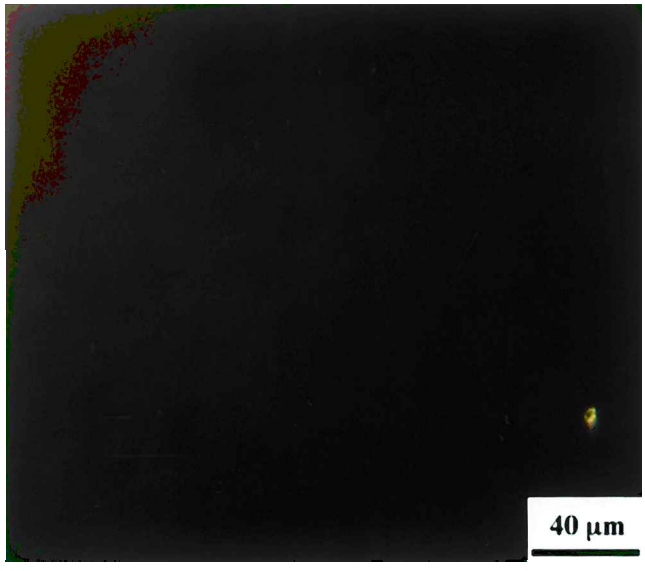

Figure 7. POM photomicrograph of the texture of the SmA phase for sample B taken at 298.2 K.

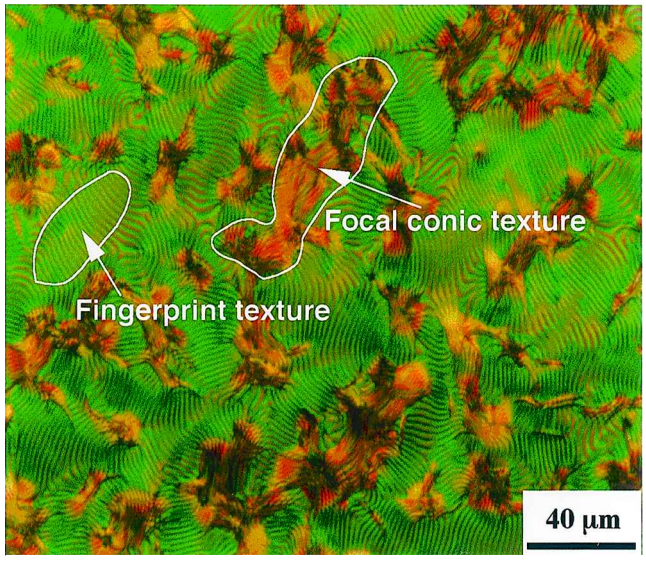

Figure 9. POM photomicrograph of the texture of the N* phase for sample B taken at 316.2 K.

difference, the optical textures of the N* phases of samples A and B were observed by POM. Figures 8 and 9 show the POM observation photographs of the N* phases for samples A and B taken at 310.2 K and 316.2 K (about 7 K above their SmA↔N* phase transition temperatures), respectively. Although the pitch lengths of the N* phases for samples A and B measured by the Cano-Wedge technique were almost the same, and the samples were prepared by the same method, the textures shown in figures 8 and 9 were remarkably different. Moreover, without being close to the SmA↔N* and the N*↔I phase transition points, both textures changed little with change in temperature in the N* phase range. It was confirmed by POM that, upon cooling sample A from N* to SmA at 1.0 or 5.0 K min^{-1}, the texture shown in figure 6 (i.e. a dark field) re-formed. Thus the SmA phase of sample A was homeotropically oriented again due to the anchoring effect of the homeotropic orientation agent coated onto the substrate surfaces. Therefore, the striking increase of transmittance at the N*→SmA transition shown in curves 3 and 4 of figure 4 corresponds to the orientation change from the molecular alignment of the N* phase to that of a homeotropic texture of the SmA phase. For the same reason, the SmA phase of sample B was also homeotropically oriented and became transparent again upon cooling from N* to SmA at 1.0 K min^{-1}.

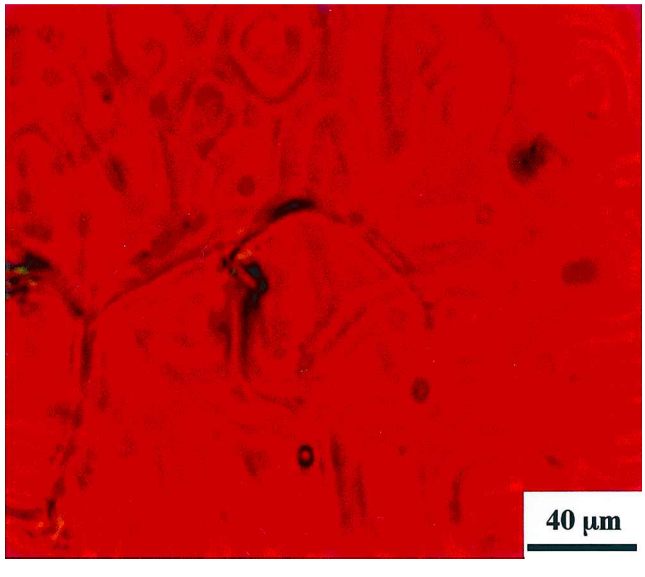

Figure 8. POM photomicrograph of the texture of the N* phase for sample A taken at 310.2 K.

However, it was confirmed by POM that a focal-conic texture, as shown in figure 10, formed in the SmA phase upon cooling sample B at 5.0 K min^{-1}. Therefore, the small increase in transmittance at the N*→SmA transition shown in curve 4 of figure 5 corresponds to the orientation change from the molecular alignment of the N* phase to that of a focal-conic texture of the SmA phase. Since sample B had the greater viscosity, it was difficult for its molecules to rearrange from the molecular arrangement of the N* phase to the homeotropic arrangement of the SmA phase. Thus, the light scattering state of the N* phase in sample B was easier to freeze into the SmA phase than that of the N* phase in sample A upon cooling at a rapid rate. Therefore, the SmA phase for sample B formed on cooling at 5.0 K min^{-1} showed strong light scattering. By using sample B, a novel TAEELCD with high contrast and stable memory effect has thus been constructed.

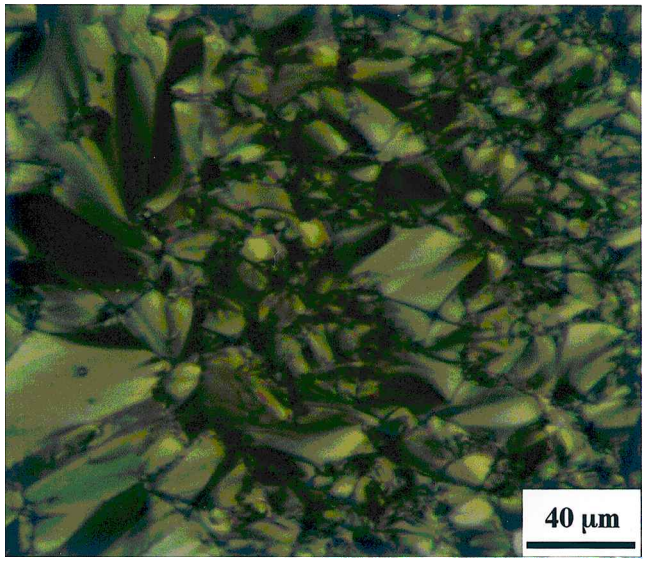

Figure 10. POM photomicrograph of the texture of the SmA phase for sample B taken at 298.2 K when formed upon cooling at a rate of 5.0 K min^{-1} from the N* phase.

It has been generally known that a N* phase can typically form four types of optical texture: (a) focal conic, (b) fingerprint, (c) planar and (d) scroll texture in POM observation under crossed Nicols [18–22]. Figure 11 shows a schematic representation of the molecular alignments of these textures. The focal-conic texture is generally obtained when polydomains are formed with their helical axes arranged in different directions. If a N* phase forms a focal-conic texture, the N* phase shows strong light scattering because of the discontinuous spatial change of the refractive indices at the domain boundaries. The stripe pattern, with the spacing smaller than one half of the pitch length of the helical structure, can be observed in each domain of the focal-conic texture. In the case of a fingerprint texture, the helical axes of all the domains are parallel to the substrate surfaces, and a stripe pattern with a spacing of one half of the pitch length of the helical structure is observed [18, 19]. If a N* phase forms a fingerprint texture, the N* phase also shows strong light scattering. Both a focal-conic and a fingerprint texture can be recognized in figure 9. The spacing of the stripe of the fingerprint texture in figure 9 was about 2.0 μm, which is close to one half of the value of the pitch length measured by the Cano-Wedge method. Therefore, the strong light scattering of the heat-induced N* phase for sample B, shown in figure 5, may be attributed to the formation of the focal-conic and fingerprint textures.

The planar texture is obtained when all the helical axes are arranged in the direction perpendicular to the substrate surfaces. In the case of a planar texture of a N* phase, the cell will be transparent for incident visible

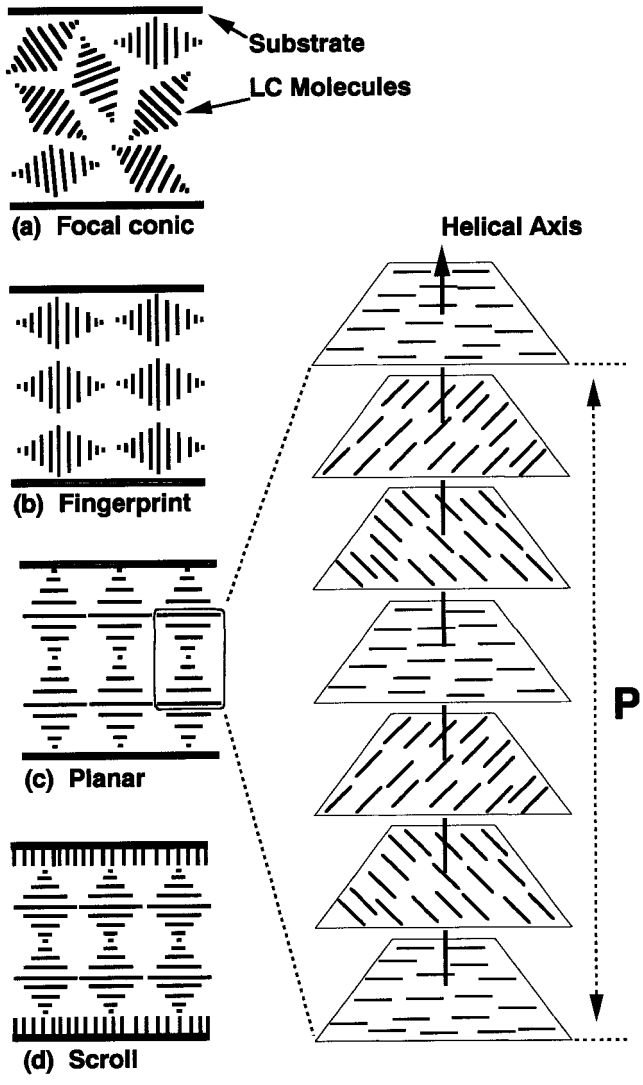

Figure 11. Schematic representation of (a) focal-conic, (b) fingerprint, (c) planar and (d) scroll textures in a N*-LC.

light in the direction perpendicular to the substrate surfaces if the pitch length is much larger or smaller than the wavelength [18, 19]. A planar texture exhibits a uniform field of bright colours under crossed Nicols, sometimes with some bright lines ('oily streaks'), resulting from defects of orientation under POM observation [19–22]. In many cases, when a thin cell whose inner surfaces have not been treated for orientation of LC molecules is filled with a N*-LC, a planar texture more easily forms and is more stable than a focal-conic texture. This is attributed to the distortion energy of the N*-LC with planar texture being smaller than that of an N*-LC with focal conic or fingerprint texture, because the planar texture has many fewer defects of molecular alignment [23]. In this case, if the inner surfaces of the cell had been treated for homeotropic alignment of the LC molecules, those in the vicinity of the substrates should

be homeotropically oriented due to the anchoring effect of the surface orientation agent, while the LC molecules in the centre of the cell take a planar molecular alignment as schematically shown in figure 11 (*d*). Thus, a scroll texture forms.

A scrolled stripe pattern can be observed in figure 8 which is clearly different from a planar texture. Moreover, since the stripe spacing is much larger than one half of the pitch length, and the N* phase of sample A in this state showed very weak light scattering as shown in figure 4, it is also different from a focal-conic or fingerprint texture. In order to identify the type of molecular alignment in this sample, the incident angle dependence of the laser diffraction of sample A in the N* phase was investigated at 310.2 K. Due to formation of the helical structure in the molecular alignment, the N* phase has spatial periodicity of the refractive indices along the helical axis. Therefore, the N* phase can operate as a diffraction grating for light. Thus, for a planar texture irradiated by a laser beam under the conditions schematically shown in figure 3, diffraction of light should occur at a certain incidence angle α ($0^\circ < \alpha < 90^\circ$) if the pitch length of the helical structure is of the order of a few μm. Then two scattered points at both sides of the direct laser beam in the vertical direction should be observable on the screen. However, no scattering points will be observed at $\alpha = 0^\circ$ in the case of a planar texture. For a focal-conic or fingerprint texture, some concentric circles appear on the screen when $0^\circ \leqslant \alpha < 90^\circ$ since for directions of the helical axes of the domains distribute randomly in the plane parallel to the cell surfaces [24]. In fact, two scattered points at both sides of the unscattered laser beam in the vertically equatorial axis have actually been observed for sample A on the screen when $30^\circ < \alpha < 90^\circ$ as shown in figure 12 which was taken when $\alpha = 45^\circ$. Moreover, no scattering points were observed for the sample when $\alpha \cong 0^\circ$. These results indicate that the direction of the helical axis in the cell of sample A in the N* state is oriented mainly perpendicular to the substrate surfaces in the cell. Furthermore, since the inner surfaces of the substrates had been treated homeotropically, the LC molecules in the vicinity of the substrates should be homeotropically oriented. Thus, the texture shown in figure 8 should be a scroll texture whose molecular alignment is schematically shown in figure 11 (*d*) [22]. That is, the LC molecules in the centre of the cell take a planar molecular alignment while those in the vicinity of the substrates are homeotropically aligned. Thus, the heat-induced N* phase for sample A exhibited weak light scattering from the boundaries between the LC molecules taking planar molecular alignment in the centre of the cell and those taking vertical alignments in the vicinity of the substrates [20–22].

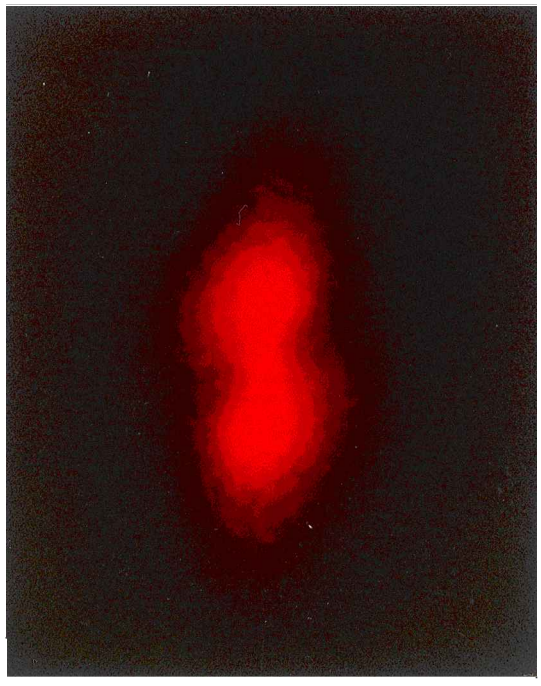

Figure 12. Photograph of the laser diffraction pattern for sample A taken at 310.2 K when $\alpha = 45.0^\circ$.

It is known that, when an appropriate electric voltage above a threshold value is applied to a N* phase forming a scroll texture, the directions of the helical axes of the domains in the centre of the cell will tend to be rotated from a direction perpendicular to the substrate surfaces to one nearly parallel to the substrate surfaces, if the dielectric anisotropy of the LC is positive [20–22]. That is, the scroll texture will be changed into a fingerprint texture by applying the electric field. Figure 13 shows the applied voltage (1.0 kHz) V dependence of the transmittance for sample A at 310.2 K, and figure 14 is a POM photomicrograph of the texture of sample A taken at 310.2 K when a voltage of 10.0 V_{rms} was applied. It is shown in figure 13 that when the applied voltage was larger than 4.5 V_{rms}, the transmittance strikingly decreased with increasing voltage. Meanwhile, a stripe pattern of fingerprint texture, with the stripe spacing approximately equal to one half of the pitch length was observed, as shown in figure 14. When the applied voltage was larger than 20.0 V_{rms}, sample A became transparent and optically isotropic because the N* phase was changed into an electric field-induced homeotropically oriented N phase. This proves further that the optical texture shown in figure 8 is a scroll texture.

From the above results, it was confirmed that the light scattering intensity of a heat-induced N* phase could be greatly improved by doping LCs with a SCLCP. It is well known that the flexible polymer backbone of a SCLCP has a tendency to form a random-coil

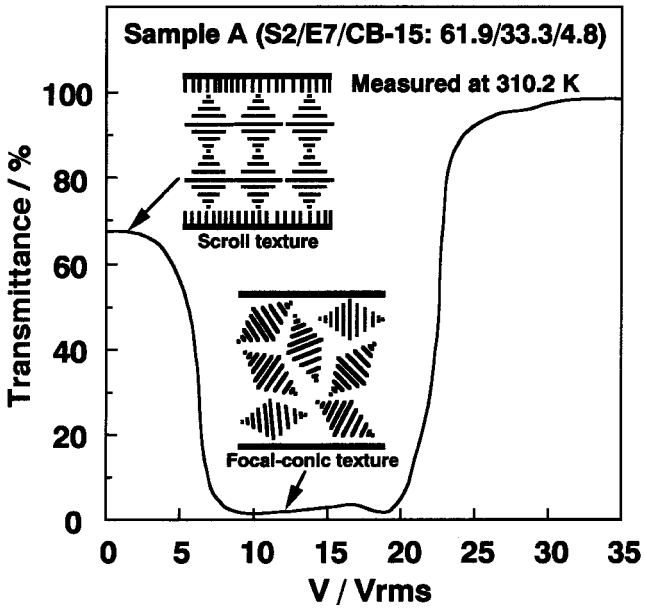

Figure 13. Plot of applied voltage (1.0 kHz) versus transmittance for the sample A measured at 310.2 K.

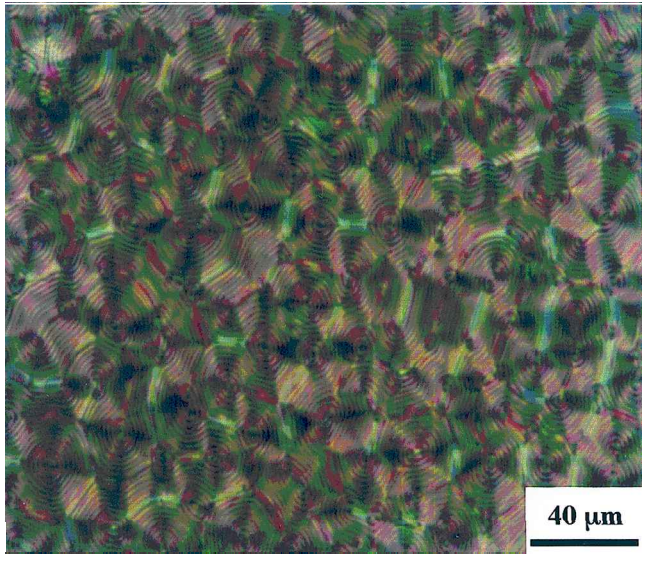

Figure 14. POM photomicrograph of the texture of the N* phase for the sample A taken at 310.2 K when a voltage of 10.0 Vrms (1.0 kHz) was applied on it.

statistical conformation. In order to form a mesogenic phase with a SCLCP, the motion of the polymer backbones of the SCLCP must be decoupled from that of the anisotropically orientable mesogenic side groups in the fluid state. The decoupling can be achieved if a flexible spacer is inserted between the polymer backbone and the mesogenic side group. However, in reality the mesogenic side groups and the polymer backbones still mutually affect the ordering, the motion and the orientation somewhat. The interaction between the mesogenic side groups and the polymer backbones can only be partially decoupled [25]. Thus, it is easy to understand that when the SmA phase of sample B is homeotropically oriented, the PS(4BC/DM) backbones are also oriented more or less anisotropically in the composite. That is, planes containing the backbones should have a tendency to be parallel to the substrate surfaces as schematically shown in figure 15(*a*). If a focal-conic or fingerprint texture formed in the N* phase after sample B is heated from SmA to N*, the formation of the helical structure in the N* phase requires no great rearrangements of the LC molecules and the mesogenic side groups of PS(4BC/DM), considering the molecular alignments of the SmA and the N* phases. Only the relative rotation around the molecular short axes of the LC molecules and the mesogenic side groups of PS(4BC/DM) in the plane perpendicular to the substrate surfaces, as schematically shown in figure 15(*b*), is necessary. Therefore, a large translational rearrangement of the backbones of PS(4BC/DM) is also unnecessary. On the contrary, if the helical axes in the heat-induced N* phase are perpendicular to the substrate surfaces like a scroll texture, a relatively greater rearrangement of some LC molecules and mesogenic side groups of PS(4BC/DM) would have been necessary, because the molecular long axes of the LC molecules and mesogenic side groups must have rearranged from a direction perpendicular to the substrate surfaces to that parallel to the substrate surfaces. Then some backbones of the

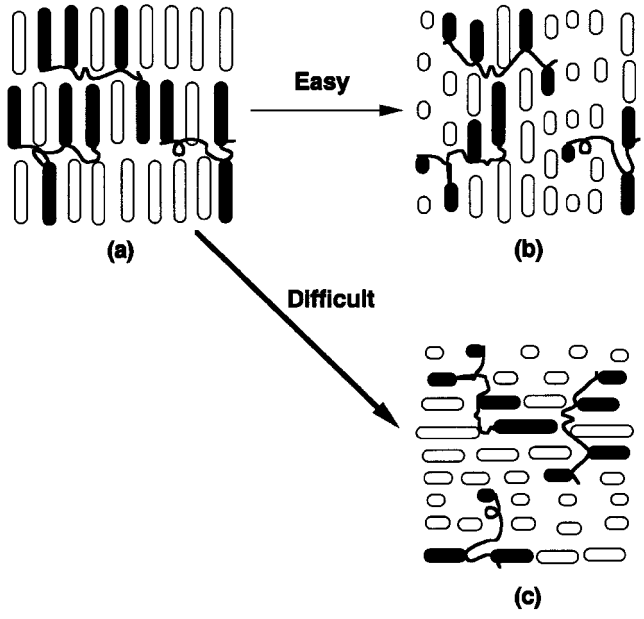

Figure 15. Schematic representation of the process of molecular arrangements accompanying the heat-induced SmA → N* transition for sample B.

PS(4BC/DM), except those in the vicinity of the substrates, must be rearranged from a state with the plane containing them tending to be parallel to the substrate surfaces to that with the plane tending to be perpendicular to the substrate surfaces, as schematically shown in figure 15(*c*).

Since sample B contains PS(4BC/DM), its viscosity is much larger than that of sample A. A large molecular rearrangement is difficult for sample B. Thus focal-conic and fingerprint textures are easier to form in the N* phase of sample B than a scroll texture. Moreover, once the focal-conic and fingerprint textures are formed, they are also very stable due to the larger viscosity. However, since sample A containing the low molecular mass substances has a lower viscosity, the molecular rearrangement from the state of the homeotropically aligned SmA phase to the scroll state of the N* phase is realized easily.

4. Conclusion

The magnitudes of transmittances began to decreased strikingly at the heat-induced SmA $\rightarrow$ N* phase transition points for both the (S2/E7/CB-15) and the [PS(4BC/DM)/E7/CB-15] composites. Since a scroll texture formed in the heat-induced N* phase of the former composite, the N* phase showed weak light scattering. However, a fingerprint and a focal conic textures formed in the heat-induced N* phase of the latter composite at the same time and the N* phase showed strong light scattering. PS(4BC/DM) had played a key role in the formation of the strong light scattering N* phase. Due to the anchoring effect of the homeotropic orientation agent coated onto the substrates, the SmA phase of the former or the latter composite was homeotropically oriented again upon cooling slowly from the N* phase. However, on cooling rapidly, the strong light scattering state of the N* phase of the latter composite was easier to be frozen in the SmA phase than that of the N* phase of the former composite due to the existence of PS(4BC/DM) in the latter composite.

References

[1] McArdle, C. B. (editor), 1989, *Side Chain Liquid Crystal Polymers* (New York: Chapman and Hall), p. 309.

[2] Kajiyama, T., Kikuchi, H., Miyamoto, A., Moritomi, S., and Hwang, J. C., 1989, *Chem. Lett.*, 817.

[3] Kikuchi, H., Moritomi, S., Hwang, J. C., and Kajiyama, T., 1991, *Polym. adv. Technol.*, **1,** 297.

[4] Kajiyama, T., Kikuchi, H., Miyamoto, A., Moritomi, S., and Hwang, J. C., 1990, *Mater. Res. Soc. Symp. Proc.*, **171,** 305.

[5] Kajiyama, T., Kikuchi, H., Hwang, J. C., Miyamoto, A., Moritomi, S., and Morimura, Y., 1991, *Prog. Pacific polym. Sci.*, **1,** 343.

[6] Hwang, J. C., Kikuchi, H., and Kajiyama, T., 1992, *Polymer*, **33,** 1821.

[7] Hwang, J. C., Kikuchi, H., and Kajiyama, T., 1995, *Polym. J.*, **27,** 292.

[8] Kikuchi, H., Kibe, S., and Kajiyama, T., 1995, *Proc. SPIE*, **2408,** 141.

[9] Kibe, S., Kikuchi, H., and Kajiyama, T., 1996, *Liq. Cryst.*, **21,** 807.

[10] Kikuchi, H., Kibe, S., Yamane, H., and Kajiyama, T., 1999, *Mat. Res. Soc. Proc.*, **559,** 75.

[11] Yang, H., Yamane, H., Kikuchi, H., and Kajiyama, T., 1998, *Mol. Cryst. liq. Cryst.*, **312,** 203.

[12] Yang, H., Yamane, H., Kikuchi, H., and Kajiyama, T., 1999, in Proceedings of the 5th International Conference on Advanced Materials, p. 426.

[13] Yang, H., Yamane, H., Kikuchi, H., and Kajiyama, T., 1999, in Proceedings of the 6th Pacific Polymer Conference, p. 354.

[14] Yang, H., Yamane, H., Kikuchi, H., and Kajiyama, T., 2000, *Liq. Cryst.*, **27,** 721.

[15] Finkelmann, H., Kiechle, U., and Rehage, G., 1983, *Mol. Cryst. liq. Cryst.*, **94,** 343.

[16] Kahn, F. J., 1973, *Appl. Phys. Lett.*, **22,** 386.

[17] Cano, R., 1968, *Bull. Soc. Fr. Mineral.*, **91,** 20.

[18] De Gennes, P. G., and Prost, J., 1993, *The Physics of Liquid Crystals* (Oxford: Clarendon Press), pp. 263–320.

[19] Blinov, L., 1983, *Electro- and Magneto-optical Properties of Liquid Crystals* (Chichester: John Wiley), p. 213.

[20] Uchida, T., Seki, H., Shishido, C., and Wada, M., 1981, *Proc. SID*, **22,** 41.

[21] Cladis, P. E., and Kleman, M., 1972, *Mol. Cryst. liq. Cryst.*, **816,** 1.

[22] Kashnow, R. A., Bigelow, J. E., Cole, H. S., and Stein, C. R., 1975, *Liquid Crystals and Ordered Fluids*, Vol. 2, edited by J. F. Johnson and S. R. Porter (New York: Plenum), p. 483.

[23] Yang, D. K., Chien, L. C., and Fung, Y. K., 1996, *Liquid Crystals in Complex Geometries*, edited by G. P. Crawford and S. Zumer (London: Taylor & Francis), p. 125.

[24] Wysocki, J., Adams, J., and Haas, W., 1969, *Mol. Cryst. liq. Cryst.*, **8,** 471.

[25] Finkelmann, H., Happ, M., Portugall, M., and Ringsdorf, H., 1978, *Makromol. Chem.*, **179,** 2541.